Spherically-expanding flames in hybrid aluminum-methane-oxidizer mixtures

James Eamon Vickery

Department of Mechanical Engineering
McGill University
Montreal, Quebec

August 15, 2017

This thesis is submitted to McGill University in partial fulfillment of the requirements for the degree of Master of Engineering.

Acknowledgements

I would like to thank my supervisors Prof. Jeff Bergthorson and David Frost for their continual support, guidance, and patience while working with me over the years. Similarly, I would also like to thank Philippe Julien, Michael Soo, Jan Palecka, Keena Trowell, and Alex Wright, not only for their support in the lab, but also our friendship that that extended well beyond the work environment and provided me with some of the wildest adventures during my time in grad school. There have also been countless undergraduates, such as Christopher Kowal, Keishi Kumashiro, Jessica Droujko, Michelle McRae, Santino Salvo, Justin Hayto, and Elie Bou-Gharios, who have provided invaluable support, allowing the Metal Flames lab to continue to function at such a a high level. And Thompson House, for always being there to help us celebrate the good and commiserate bad over the years. This thesis would not have been possible without all of you.

To my parents, Jay and Trish Vickery, thank you for all of your support over the years. From a young age you instilled the importance of education in me and have continued to push and support me in all of my endeavors, academic and others, while also being excellent role models who constantly display discipline, dedication, and love in your everyday lives.

I would also like to thank the McGill Redmen Lacrosse team for all the great years, especially the undefeated 2015 season. Thanks for letting this old man finally get the ring that eluded me all of these years.

And finally, I would like to give a shout out to Club 1211 and all of its constituents: Co-founder Billz Trepagnier, resident DJ Mark-e-Mark, Big Zed, Sean Half-man-half-amazing Haffey, Randy Pytelins, Scott Ferguson, Julian Harrison, Bignut, Adam. Peterson., Mr. Makoto, Mr. Birch, Jerome Miles, and Glen Lui. We may have moved out the basement years ago, and our constituents have now spread across the globe, but the club lives on in our hearts and minds.

Abstract

The propagation of constant-pressure flames through hybrid aluminum-methane-oxidizer mixtures in transparent latex balloons is investigated using high-speed cameras that record both the dust dispersal and the subsequent spherical flame propagation processes. For mixtures without excess oxygen in the post-methane flame zone, the aluminum acts only as an inert diluent at low concentrations, resulting in a decline of the flame speed with aluminum concentration. Past a critical concentration around 100 g/m^3, the flame speed stops decreasing and remains constant with increasing aluminum concentration, a behavior which is attributed to the formation of a high-temperature aluminum flame front that thermally couples to the methane flame. When there is excess oxygen to react with the aluminum, the flame speed monotonically increases with aluminum concentration before reaching a plateau at aluminum concentrations above 150 g/m^3. The difference in behavior at low concentrations in mixtures with and without excess oxygen is explained by the ability of aluminum particles reacting with free oxygen to ignite and burn in the diffusion-limited combustion mode. The igniting particles are able to form high-temperature micro-diffusion flames which attain high combustion rates even at the relatively low bulk gas temperatures typical for methane flames.

Abrégé

La présente thése porte sur l'étude de la propagation isobarique de flammes dans des mélanges hybrides d'aluminium et de méthane. Les mélanges sont contenus à l'intérieur de ballons transparents en latex et la dispersion de la poudre, ainsi que les flammes, sont filmées à l'aide d'une caméra á haute vitesse. Dans les mélanges comburant-carburant sans surplus d'oxygéne après la flamme de méthane, l'aluminium en faible concentration agit en tant que diluant, ce qui a pour effet de réduire la vitesse de la flamme de méthane. Au-delá de 100 g/m^3, la célérité de flamme demeure constante avec la concentration d'aluminium. Une flamme d'aluminium se forme ainsi á haute concentration et échange de la chaleur avec la flamme de méthane. Lorsqu'il y a un surplus d'oxygène aprés la flamme de méthane, la célérité de la flamme de méthane augmente avec une augmentation de la concentration d'aluminium avant d'atteindre un plateau au moment oú la concentration d'aluminium atteint 150 g/m^3. Cette différence de comportement dans les mélanges avec surplus d'oxygéne s'explique par la capacité des particules d'aluminiums d'initier la combustion en mode diffusion avec l'oxygène disponible. Une micro-flamme se crée autour de chaque particule et produit des températures supérieures aux températures de la flamme de méthane.

Contents

List of Figures

List of Tables

1 Metals in reactive systems

Metals have large energy densities [1,2], and the addition of metals to reactive systems often increases the energy density of the mixture and can lead to an increased energy output of these systems. For example, metals such as aluminum and magnesium are commonly added to rocket propellants [3] and explosives [4,5] where they burn in the products of the initial explosive in order to increase the specific impulse or blast wave pressure. Metal powders are also frequently encountered in industrial settings where there may also be volatile liquid or vapor fuel sources present [6,7]. In the case of an accidental explosion, the metal powder and combustible gas can mix and together react in the surrounding air. Over the years, most of the work studying the combustion of these metal powders have focused on determining when and how the metals burn within these different reactive systems.

Metals are often lumped into the category of combustible dusts, but there is a wide variety of combustible dusts with different physical characteristics. Coal and organic dusts contain a significant amount of volatile components which evaporate in the flame pre-heat zone and mix with the surrounding air, which can lead to a continuous flame sheet in the reaction zone while the solid char burns heterogenously in a secondary reaction zone [8]. Flames propagating in suspensions of dusts with appreciable volatile material can even be modeled similarly to gas flames [9]. Plastics have low melting and boiling temperatures compared to their flame temperatures, leading to significant evaporation in the pre-heat zone with their combustion resembling that of liquid droplets [10]. Metals, on the other hand, have much higher boiling temperatures compared to their flame temperatures. Therefore, even for metals with flame temperatures above their boiling temperature that burn in the vapor-phase, there is no significant evaporation in the flame pre-heat zone. Furthermore, metal vapors are extremely reactive with very low activation energies which precludes the accumulation of unreacted metal vapor in the pre-heat zone [11,12]. Additionally, plastic and organic dusts are competing for the same oxidizers as hydrocarbons, and the addition of these dusts has little effect on the energy content of stoichiometric and fuel-rich hydrocarbon mixtures [13]. Metals, on the other hand, can react with the products of hydrocarbon flames (i.e. steam and carbon dioxide), and the addition of metals to hydrocarbon fuels significantly increases the energy density of the hybrid fuel mixture. Thus it is necessary to study hybrid mixtures of metal-hyrdrocarbons separately.

1.1 Fundamental considerations of metal combustion

There are two main processes that control the burning of particles [14, 15]. The first is the diffusion of oxidizers to the particle surface, and the second is the reaction at the surface between the particle and the oxidizer. These two successive processes lead to two asymptotic combustion regimes where the rate-limiting step of the reaction is either the diffusion of oxidizer to the particle (diffusion-controlled regime) or the kinetic rate of reaction at the particle surface (kinetically-controlled regime), with each regime having its own distinct characteristics.

In the diffusion controlled regime, the oxidizers are consumed faster than they can be transported to the particle, leading to an oxidizer concentration gradient between the particle surface and the surrounding gas. Similarly, the production of heat from the reactions at the particle surface is faster than the rate at which it can be transported away, leading to the particle being at a locally higher temperature than the surrounding gas. In the kinetically-controlled regime, the rate of transport is sufficiently fast, and there are no gradients of temperature or species. An illustration high-lighting key features of the diffusion-controlled and kinetically-controlled regimes are shown below in Fig. 1.

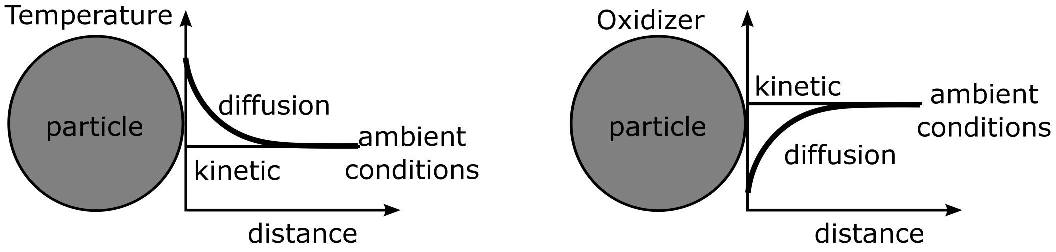

Figure 1: Temperature and oxidizer contration profiles for diffusion-controlled and kientically-controlled particle combustion.

When the particle initially begins to react, the particle burns in the kinetically-limited regime. As the particle starts reacting, energy is released as heat, and if the rate of heat generation is greater than the rate of heat loss to the surroundings, the particle will transition from kinetically-limited to the diffusion-limited regime. This transition from kinetically-limited to diffusion-limited is defined as particle ignition and is analoguous to Semenov thermal ignition theory [15, 16].

1.2 Early work: single particle experiments

In the late 1950s and early 1960s, the interest in metal combustion in the scientific community increased due to the increased prevalence of metallized propellants and explosives [3, 8]. In these systems, the metals burn in the hot combustion products of the initial propellant or explosive where it reacts primarily with water, carbon dioxide, and any oxygen remaining in the gas. In order to improve performance (combustion efficiency, reduction in slag formation), more fundamental knowledge on the burning of metal particles was needed.

Glassman [8] was one of the first to work on this problem. He recognized that the combustion of metal particles would be similar to what had been seen in droplet combustion and proposed that the combustion is controlled by diffusion of oxidizer to the particle. In this diffusion-controlled regime, the time it takes for the particle to burn completely, subsequently referred to as the particle burn time and denoted as τ, depends on the initial particle diameter, denoted as D, according to the following relationship: $\tau \propto D^2$ [17].

Unlike droplets, however, metals tend to have much higher boiling temperatures compared to their flame temperatures [1], and whether they react in vapor-phase or heterogeneously depends on the specific metal. Some metals, such as aluminum [18] and magnesium [19], have flame temperatures above their boiling temperatures, which leads to vapor-phase metal-oxidizer reactions. Other metals, such as iron [20] and zirconium [21], have flame temperatures below their boiling temperatures, and the reaction takes place between the gaseous oxidizer and the molten metal on the particle surface. This criteria, known as the Glassman criteria, was confirmed by Brzutowski and Glassman [22] while performing experiments on burning strands of aluminum, magnesium, and zirconium. Aluminum and Magnesium atomic vapor lines were observed in emission, indicating the existence of metal vapor in the flame. In the zirconium tests, there was no evidence of metal vapor. Furthermore, aluminum and magnesium emission lines also showed evidence of self-absorption. This is indicative of two temperatures in the flame, with high temperature emission in one part of the flame, and low temperature absorption in the other, which suggests that the metal is burning in the diffusion controlled regime with a lifted vapor diffusion flame. Many other early efforts also observed lifted vapor-diffusion flames with aluminum and magnesium particles [23–27].

Most experimental efforts in the early 1960s and 1970s focused on the combustion of single, isolated particles. Due to their relevance in engineering systems, some of the first experiments performed were propellant ignited combustion experiments [23, 28] where metal particles were observed burning in the products of an initial low-explosive. An improvement to this technique is the gas-flame initiation technique [24, 25, 27, 29] where the metal particles are injected into the hot flow from a gas-burner. Using different gaseous fuels, such as methane, carbon monoxide, and hydrogen, at various equivalence ratios allowed for more precise control of the combustion environment [27, 29, 30]. Experiments where the particles are laser-ignited [26, 28, 31–34] or shock ignited [35–37] led to further improvements. These techniques allow for complete control over the initial temperature, pressure, and oxidizer type and concentrations, unlike in the propellant and gas-flame ignited experiments which require a primary reaction front to provide the conditions necessary to initiate the reaction.

These studies often measured parameters such as ignition temperature [24, 25], ignition delay time [23, 28, 29], and the particle burn time [18, 23, 25, 26, 29, 30]. The particle burn time was measured as a function of initial particle diameter in several cases. The relationship most commonly found was $\tau \propto D^{1.8-1.5}$, which is different from the $\tau \propto D^2$ predicted by Glassman [8]. The difference is attributed to the metal oxide condensing on the particle surface, which limits the surface area available for reaction, whether the reaction be heterogeneous oxidation of evaporation of the metal.

Due to limitations in experimental and imaging techniques, many of these initial tests were carried out using particles larger than 50 microns, and the particles were observed burning in a diffusion-limited regime. In practical situations, smaller particles are desired. Due to their increased specific surface area, there is promise for increased reaction rates and reduced slag formation [36]. Some researchers have tried to extrapolate burn times of small particles using correlations developed from experiments with large particles [18]. This is problematic as the combustion regime will shift from a diffusion-controlled regime to a kinetically controlled regime as the particle size decreases where the burn time of a particle is theoretically $\tau \propto D$ [36]. For particles that burn a significant amount of mass in the kinetically-limited regime, predictions from these correlations dedcucded from exepriments with large particles may yield erroneous results. Some of the more recent efforts have specifically focused on smaller particles, investigating the particle mode of combustion, and determining where the transition from the diffusion to kinetic regime occurs [31, 32, 35, 36].

Different spectroscopic techniques are typically used to investigate the particle mode of combustion. Identification of certain species or different temperatures in the system can be used to determine the mode of combustion. Glumac and his group [35, 36] used emission spectra and three color pyrometry to identify different temperatures in the flame in order to determine the transition from diffusion-controlled to kinetically-controlled combustion. Results show that the regime of combustion depends not only on the size of the particle, but on the available oxidizers, ambient temperature, and ambient pressure. In the case when aluminum was found be burning in the kinetically-limited regime, the temperature of the reaction was at the aluminum boiling temperature, indicating that the limiting kinetic rate for aluminum combustion is the evaporation of the aluminum vapor from the particle surface [36].

1.3 Metals reacting within a suspension

One of the key limitations of single particle experiments is that, in any practical system, combustion of metal powders in these reactive systems occurs in a dense suspension of particles. When this occurs, heat generated from the reacting particles diffuses upstream, heating the unreacted mixture and initiating new reactions, creating a self-propagating reaction wave that is called a flame. In a suspension of particles, the heat production and oxidizer consumption continuously alters the local combustion environment as the flame propagates through the mixture. In single particle experiments, the heat produced and oxidizers consumed are negligible. Consequently, results from single particle experiments may not be representative of how the particles will react in the dynamic environment of a flame.

Soo et al. [38] and Julien et al. [39] studied hybrid aluminum-methane-air flames on a Bunsen burner, a model system used to simulate conditions in rocket propellants. They found that there was a critical concentration below which the aluminum acted only as an inert additive, and above which an aluminum flame front formed and stabilized to the methane flame. Julien et al. [20] produced a follow-up piece where he investigated iron-methane-air flames and also observed the same critical concentration behavior, showing that this behavior is not specific to a type of metal, but is instead an inherent feature of these hybrid metal-powder/combustible-gas systems. The results from this work go against the common assumption that particles must be heated to an ignition temperature in order to react. Many flame models use parameters such as ignition temperature and particle burn time to predict how the particles will burn. In the experiment, the addition of metal powder reduces the methane flame temperature, and models using ignition temperature would predict that the metal would therefore be less likely to react as the metal fuel concentration in increased. The results show, however, that the collective effects of particles reacting and releasing heat can lead to rapid combustion of the suspension compared to the combustion of a single particle put in the same oxidizing environment.

Palecka et al. [40] also observed the critical concentration behavior found by Soo [38] and Julien [39] while studying flames in hybrid aluminum-methane-air mixtures propagating in tubes. He further analyzed the structure by measuring the quenching behavior of these hybrid mixtures. The results from this work indicate that there are two different coupling regimes: one where the aluminum and methane flame zones are separated and one where the two flame zones are overlapped.

Denkevitz et al. [41] studied hybrid hydrogen-aluminum systems using a constant volume combustion bomb. He found that, at low concentrations of metal concentration, the explosion took place in one stage with pressure data similar to the hydrogen case without dust. As the concentration was increased, the explosion took place in two stages with two distinct pressure rises. As the concentration was further increased, the two peaks eventually merged with one steep spike in pressure. While these results seem to suggest the existence of two flame fronts [41], limited scientific conclusions can be drawn in the combustion bomb apparatus due to lack of visualization of the dust dispersion and flame propagation processes.

1.4 Present work objectives

While the work performed by Soo et al. [38] and Julien et al. [39] on the Bunsen burner provide important information about how metal and gaseous fuels can interact, the stabilized configuration may not represent the full range of behavior that may exist in transient, freely propagating flames, which are inherent features of explosions. While the work done by Palecka [40] studying flames in tubes did look at freely-propagating flames, the experiments were performed with both ends of the tube open, and, in this case, the expansion of the hot gas behind the flame does not influence the flame propagation. In an outwardly propagating flame, however, the expansion of the hot gases pushes on the flame, leading to a much faster rate of propagation. This is particularly important in explosions of systems with different types of fuels where secondary reactions behind the primary front may increase the amount of expansion and, thus, the propagation speed.

While the geometry of the combustion bomb experiments allows this effect to be studied, the diagnostic methods to investigate the flame in the vessel are limited. Due to the high pressures generated in the vessel during the experiment, high strength materials are needed, limiting the visual access. Without this visual access, assessing the dust dispersion process and the cloud uniformity is difficult. Large gradients in concentration and limited information about particles depositing to the walls adds to the uncertainty of the measurements. Furthermore, the main diagnostic tool used is the pressure vs time trace, which only provides information about the flame when it is close to the vessel wall, and, therefore, any unsteady behavior cannot be detected. Instabilities arising from hydrodynamic effects, thermodiffusive effects, and acoustic interactions with the vessel wall may cause the flame to accelerate, and thus the measurements made for the same mixture could yield different results depending on the size of the vessel used.

In order to overcome the shortcomings of these previous works when assessing the role of metal addition to hydrocarbon fuel mixtures for outwardly-expanding flames, the present work uses balloons to contain the dust-combustible gas mixture. This experimental method, which was recently introduced in previous work [42, 43], allows for spherically propagating flames in hybrid mixtures to be visually observed at multiple stages during the propagation. The use of clear latex balloons provides a constant-pressure combustion environment while also permitting visual access. High-speed cameras are used to record not only the flame propagation but also the dust-dispersal process, enabling the assessment of the cloud uniformity at the time of ignition.

The objective of the present work is two-fold. The first is to analyze under what conditions the metal particles will become reactive in the system, specifically focusing on both the roles of available oxidizers and metal fuel concentration. The second is to study the different metal-pwoder/combustible-gas fuel interactions that can occur in freely-propagating flames where the effect of gas expansion significantly influences the flame propagation compared to the stabilized flame configurations. This work uses the exact same batch of aluminum powder that was used previously in the Bunsen flame [38, 39] and quenching tube experiments [40], which allows for meaningful comparison between the different geometric configurations.

2 Experimental methods

2.1 Experimental set-up

Experiments are performed in transparent latex balloons measuring approximately 30 cm in diameter. The balloon is initially inflated with the desired combustible-gas mixture, after which the dust is dispersed within the balloon by a 0.8 s pulsed flow of the same gaseous mixture. A delay of 4 s is introduced between the end of the dust dispersal process and ignition to allow turbulence to decay [43]. The mixture is ignited in the center of the balloon by a tungsten wire of 50 micron diameter that is rapidly heated by the discharge current from an electrolytic capacitor. In order to enable the self-formation of an aluminum dust flame, as has been observed in previous work [38–40], the igniter chosen in the present experiments is only energetic enough to initiate the gaseous methane flame and would be insufficient to ignite the combustible dust mixture. As the flame propagates outwards, the balloon expands, maintaining an approximately isobaric environment, and bursts when the flame reaches the balloon surface. Figure 2 shows a picture-schematic of the apparatus along with still frames of the dust-dispersal and flame-propagation processes. Additional schematics of the apparatus with more detailed descriptions are given in previous publications [42, 43].

The present experimental configuration presents many advantages over rigid constant volume-combustion bombs for the study of spherically-expanding, freely-propagating flames. The transparent latex balloons allow for the study of constant pressure systems and provide full visual access that allows the flame symmetry and dust cloud uniformity to be assessed. The transient flame propagation is filmed from soon after ignition until the balloon bursts, which allows for a longer monitoring time in comparison to combustion bombs where the significant pressure rise is only observed when the flame is already close to the walls of the vessel and, therefore, any transient or unsteady flame behavior remains undetected.

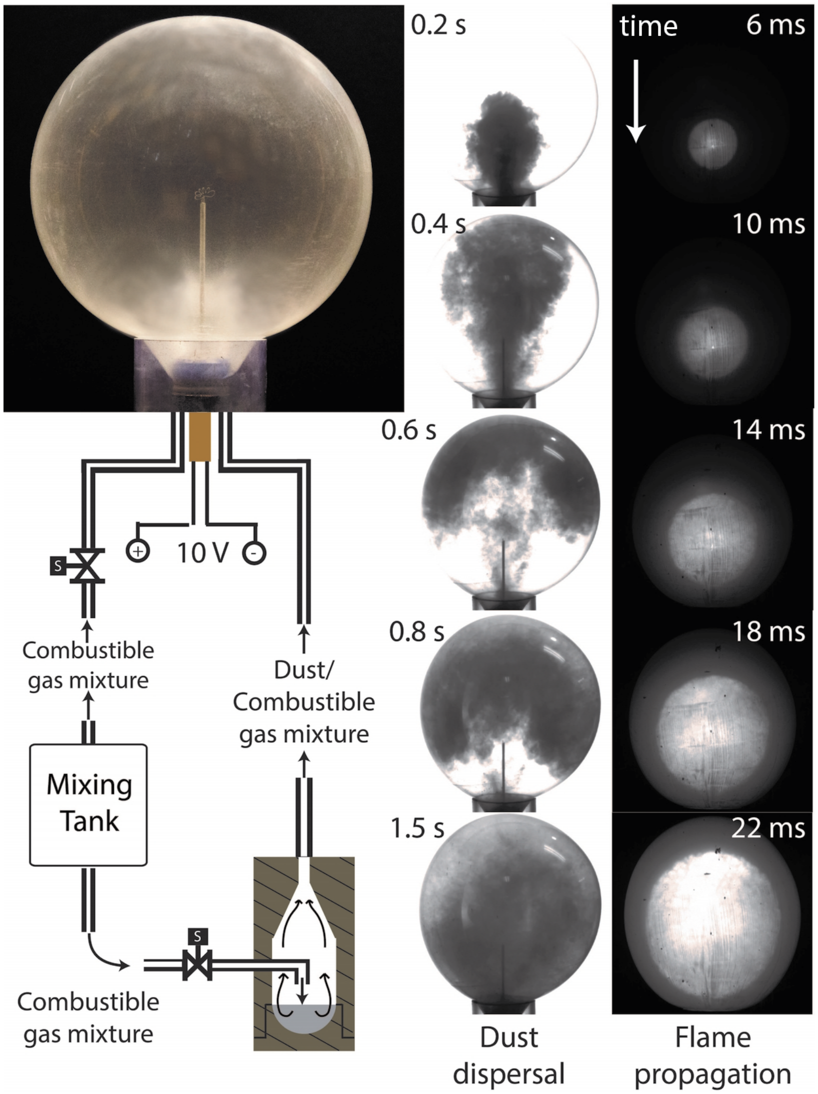

Figure 2: The left side of the figure shows the experimental apparatus with an actual picture of the inflated balloon containing only the combustible-gas mixture before dust dispersion with a schematic of the key components below. The right side of the figure shows both the dust dispersal and flame propagation processes for an 8% excess oxygen mixture and a concentration of 100 g/m^3 of aluminum.

2.2 Combustible gas mixtures

Three different gas mixtures are studied in the present work. The first gas mixture is methane-air with an equivalence ratio of 1.1, meaning there is no oxygen left in the methane flame products (0% excess oxygen). The second mixture is 26% oxygen/74% nitrogen and methane with an equivalence ratio of 0.8 (5% excess oxygen), and the third mixture is an oxidizing mixture of 30% oxygen/70% nitrogen and methane with an equivalence ratio of 0.7 (8%excess oxygen). Consequently, all of the mixtures have nearly the same flame temperature (2250 K) and thermal diffusivity which allows the effect of oxygen concentration to be isolated. A table summarizing the gas mixtures in below in Table 1.

Table 1: Combustible gas mixture properties

% O_2	% N_2	% CH_4	ϕ	% Excess O_2	T_{ad} (K)	Thermal Diffusivity (m^2/s)
18.8	70.8	10.4	1.1	0	2250	2.25
23.8	65.8	10.4	0.81	5	2250	2.24
27.8	61.8	10.4	0.7	8	2250	2.24

2.3 Dust concentration measurements and flame visualization

The aluminum powder used is Ampal 637 (Ampal, NJ), with a Sauter mean diameter of 6.5 microns. The same batch of Ampal 637 has been used in previous experiments investigating both aluminum-oxidizer and hybrid aluminum-methane-oxidizer mixtures [38–40,42,43]. Since powder dispersion and burning characteristics are largely dependent on the exact type of powder used, general comparison with results present in the literature is difficult; however, by using the same batch of aluminum powder for different experiments, the role of different geometries on the combustion characteristics can be more meaningfully compared. Experiments are also conducted with inert spherical alumina powder made by Advanced Materials with a mean particle diameter of 5 microns in place of reactive aluminum powder. Scanning Electron Microscope (SEM) photographs of the powders are shown below in Fig 3. The gaseous mixtures are seeded with powder concentrations ranging from 0-250 g/m^3. Above 250 g/m^3, the multiple scattering from all of the powder in suspension and deposited on the balloon wall does not allow for accurate tracking of the flame front.

The dust concentration in suspension at the time of ignition is obtained from a calibration performed within an acrylic sphere having the same size as the balloon [43]. Using a laser-light attenuation probe calibrated for the same powder [38], a relationship between the mass

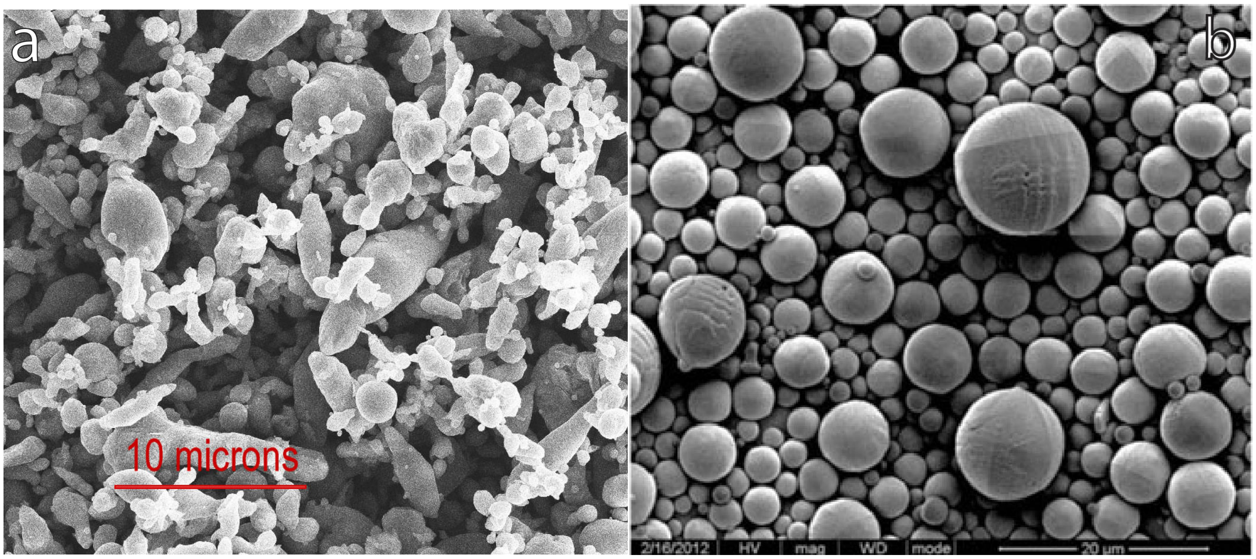

(a) (b)

Figure 3: SEM photographs of a) Ampal 637 aluminum powder and b) Advanced Materials alumina powder

placed in the powder dispersion unit and the actual concentration of powder in suspension at the time of ignition was determined. It was found that the actual concentration in suspension at the time of ignition is about 40% less than the estimate that assumes that all the powder sample is in suspension [43]. Most of this loss is from the powder depositing on the balloon wall. The strong turbulence induced from the dispersion helps to keep the particles in suspension, and the loss of powder from settling is minimal. Details on this procedure can be found in [43].

The flame propagation is recorded at 4,000 − 7,500 frames per second using a Photron SA-5 video camera. The lensing effect from the latex balloon is found to be negligible and does not affect the measurements. The position of the flame front is tracked from high-speed movies by fitting an ellipse to the flame front contour at different stages during the propagation. The radius of the flame is taken to be the average distance from the flame contour to the center-of-mass of the ellipse. The flames are analyzed over an approximate radial range of 30 mm to 100 mm, which correspond, to the minimum and maximum observable flame sizes, respectively. At radii below 30 mm, there is too little light to define the flame front, and beyond a radius of 100 mm the flame starts to interact with the balloon wall and is no longer freely-propagating. In order to analyze the flame surface topology, the high-speed videos are also processed by subtracting two subsequent images. This allows for changes in the flame surface from frame to frame to be amplified.

3 Results

3.1 Evolution of flame surface topology

Two typical results of the flame surface evolution with low dust concentrations for mixtures with and without excess oxygen are shown in Fig. 4. In the case where there is no excess oxygen (Images a, b, and c), the flame surface remains relatively smooth during propagation. The few large cells that can be observed are likely formed from the residual turbulence in the flow at the time of ignition or the asymmetric ignition device. These cells do not appear to grow during the observed propagation time. In contrast, the flame in the mixture with excess oxygen (images d, e, and f) has a corrugated and wrinkled surface during the entire observed propagation within the balloon. While only images from experiments with 8% excess oxygen are shown here, corrugated flame structures, identified as cellular flame instabilities, are also observed in the 5% excess oxygen case. Furthermore, the same behavior is observed when aluminum is replaced with inert alumina powder.

3.2 Evolution of flame radius

Three typical measurements of the evolution of the flame radius as a function of time are shown in Fig. 5 for methane-oxygen-nitrogen-aluminum mixtures having 0%, 5% and 8% excess oxygen with approximately 100 g/m^3 of aluminum in suspension. As can be seen, flames in mixtures with 0% excess oxygen display constant propagation speeds, whereas flames in mixtures with excess oxygen are accelerating. The acceleration in Fig. 5 is determined by fitting the radius vs time data to a second order polynomial and taking the second derivative of this function and is, therefore, an average value over the observed propagation. The ac-

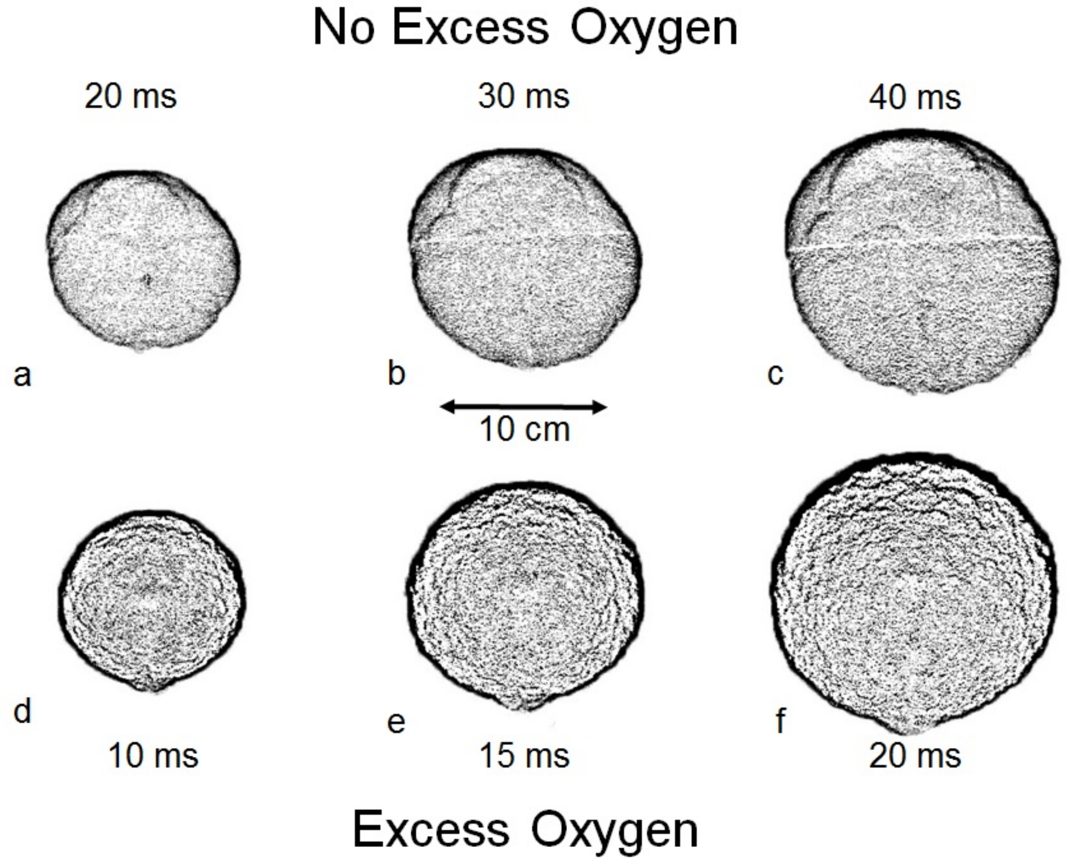

Figure 4: The top sequence of images shows the flame surface in the gas mixtures with no excess oxygen. The bottom sequence of images shows the flame surface for gas mixture with 8% excess oxygen. Both mixtures have aluminum concentrations of approximately 15 g/m^3.

celerating flames also correspond to the flames that display a cellular structure on the flame surface in Fig. 4. Furthermore, the values of acceleration show similar trends in mixtures with both inert alumina and reactive aluminum.

3.3 Flame speed measurements

The formation and growth of cells on the flame surface increase the area available for reactions, which in turn causes the flame to accelerate. In order to obtain the flame speed of the laminar, unperturbed flame (i.e. non-cellular flame), the radius vs time data for these accelerating flames are fit to the equation:

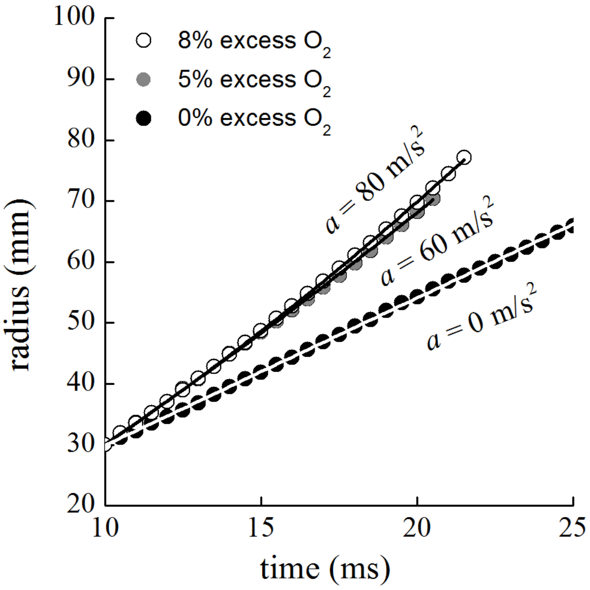

Figure 5: Radius-time flame trajectories illustrating both steady (a = 0) and unsteady (a > 0) propagation.

$$R = R_{\mathrm{c}} \left(\frac{S_{\mathrm{F}} t}{R_{\mathrm{c}}} \right)^{\alpha} \tag{1}$$

for $R > R_{\mathrm{c}}$. This expression has been used in the literature to describe the fractal growth of initially laminar methane and propane flames at atmospheric pressure [44–46]. The justification for using this expression is discussed in further detail in section 4.1. In this expression, R_{c} is the critical radius for the onset of cellular instabilities, S_{F} is the flame speed of the unperturbed spherical laminar flame, and α is related to the fractal dimension of the cells (α=1 corresponds to stable flame propagation). By fitting the data of the accelerating, cellular flames to this functional form which accounts for the acceleration due to the fractal growth of cells on the flame surface, the non-cellular flame speed, S_{F}, can be extracted, and the effect of particles in suspension can be separated from the effects of the cellular instability. In the present experiments, the results consistently show that $R_{\mathrm{c}} = 20 - 40$ mm with no trend with concentration, making the use of this equation valid for the observed flame data. Steadily-propagating flames are processed by linear regression of the radius vs time data.

The results for flame speed are shown on Figures 6a and 6b. The dashed lines on the

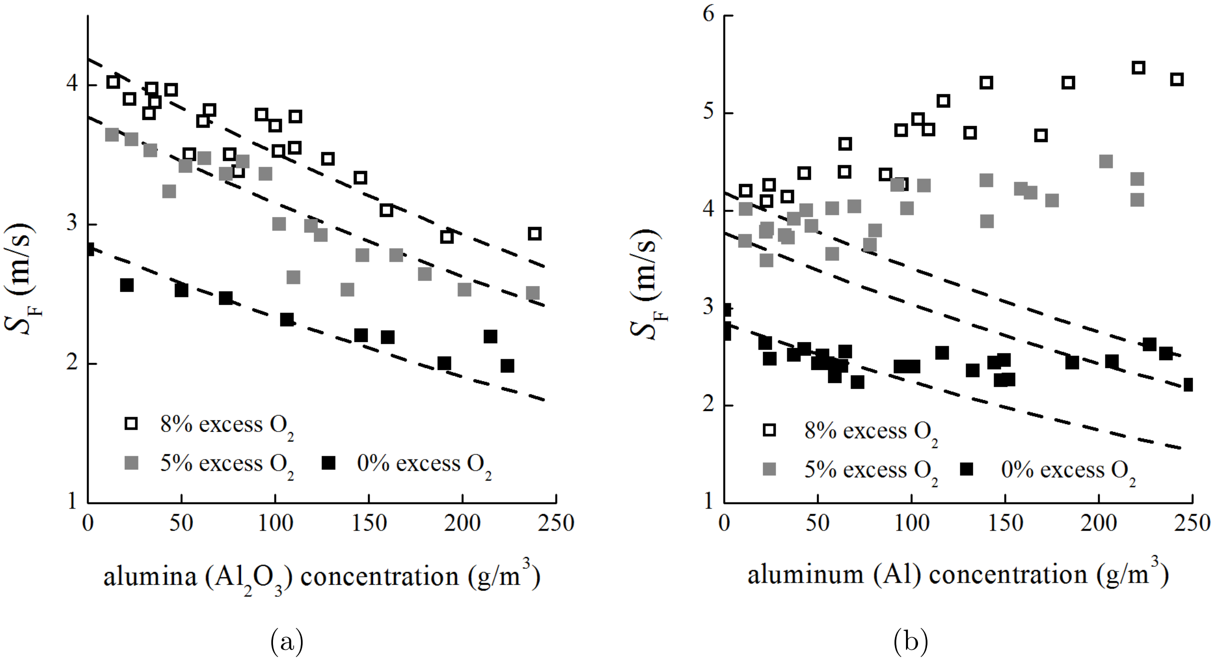

Figure 6: Flame speed measurements for a) inert alumina powder and b) aluminum powder in different gaseous mixtures. Dashed lines are theoretically calculated flame speeds assuming the alumina/aluminum is an inert additive.

graph represent the methane flame speeds calculated theoretically using the chemical kinetic software Cantera [47], assuming both alumina and aluminum powders are inert and act only as heat sinks in the flame. The effect of dust concentration is modelled by increasing the heat capacity of the mixture without changing its molecular composition. The flame speed taken from Cantera is the speed of the hot combustion products leaving the flame, which, to first order, is what is observed in spherically-expanding flame experiments.

The results from the different mixtures seeded with inert particles show good agreement with the values calculated with Cantera (see Fig. 6a). The good agreement between the predictions from Cantera and the S_{F} values extracted from the cellular flame data in mixtures with excess oxygen indicates that the fractal-growth correlation (Eq. 1) provides a good description of these flames. Simply taking an average flame speed over the observed range results in the reported flame speeds being higher than the flame speeds predicted by Cantera.

The experimental results for the mixtures with aluminum show different trends depending on whether or not there is excess oxygen in the post-methane flame zone, as shown in

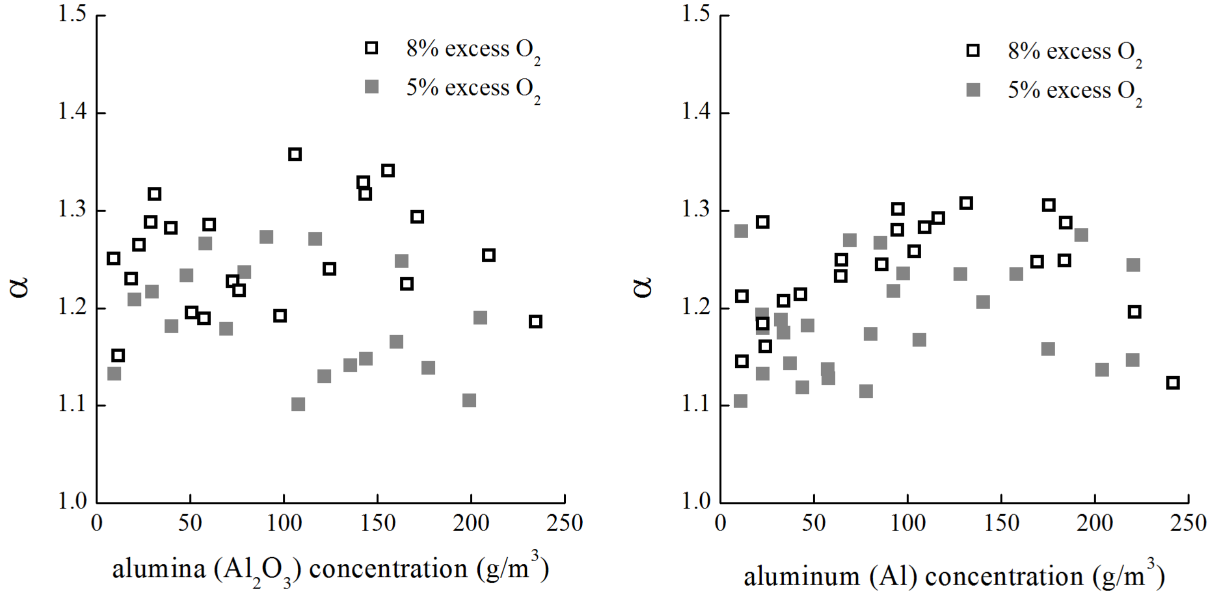

(a)

(b)

Figure 7: Values of α found by fitting the radius vs time data to the equation: $R = R_c \left(\frac{S_F t}{R_c}\right)^{\alpha}$

Fig. 6b. When there is no excess oxygen, the flame speed initially decreases with increasing aluminum concentrations, following the dashed line. After a critical concentration of about 100 g/m^3, the flame speed remains constant with increasing aluminum concentration, deviating from the dashed line predicted for inert loading. When there is excess oxygen, the flame speed monotonically increases with increasing aluminum concentration before also reaching a plateau for concentrations above 150 g/m^3.

3.4 Growth coefficient measurements

The growth coefficient, α, for the accelerating flames is plotted in Fig 7b. The results show that α remains approximately constant with increasing dust concentration, with values consistently between 1.1 and 1.3 for both inert alumina and aluminum powders.

4 Discussion

4.1 Conditions for flame stability

All spherically-expanding flames eventually become cellular at some critical radius [44–46, 48–51]. At the critical radius, the spontaneous formation and subsequent growth of cells on the flame surface cause the flame to accelerate. The cells increase the surface area of the flame, which allows the flame to propagate at a faster speed than if the flame remained smooth. As the cells grow and multiply, the surface area further increases, causing the flame to accelerate.

There are four main parameters which determine the critical radius at which a laminar flame becomes cellular: flame thickness (δ_{t}), activation energy (E_{a}), Lewis number (Le), and expansion ratio across the flame (σ). Betchold and Matalon analyzed the influence of these different parameters and found that the critical radius for the onset of cellular instabilities depends on these parameters as follows: $R_{\mathrm{c}} \propto \delta_{\mathrm{t}} E_{\mathrm{a}} \frac{Le - Le^{*}}{\sigma^{2}}$ [50, 51]. In this expression, Le^{*} is the critical Lewis number less than unity such that the flame is cellular upon ignition. In the present experiments, when oxygen replaces nitrogen in the mixture, the expansion ratio and activation energy stay the same, but the flame thickness and Lewis number are decreased.

Flames of stoichiometric and fuel-rich methane-air flames have values of the critical radius on the order of 12-20 cm [44, 45, 48, 49], which is beyond the range that the flames are observed in the present experiments; hence, no cellular flame structures, or the corresponding acceleration, are observed for these mixtures. When oxygen replaces nitrogen in the mixture, the reaction rates increase, and the flame thickness decreases. Furthermore, the addition of excess oxygen changes the mixture from slightly fuel-rich to fuel-lean, thereby changing the limiting reactant to methane which has a lower molecular weight than the average molecular weight of the mixture, causing the Lewis number to decrease to less than unity and bringing it closer to Le^{*}. Both of these effects reduce the critical radius for the onset of instabilities, resulting in the observed cellular flames for mixtures with excess oxygen. The particles in suspension may also reduce the critical radius for the onset of instabilities, similar to what has been reported for flames propagating through aerosol mixtures [52]; however, the observed acceleration appears to be primarily due to instabilities in the methane flame, as no cells were observed for mixtures without excess oxygen with variable particle concentrations. Moreover, the values of the growth coefficient, α, reported in the present work are consistent for experiments with both inert and reactive powders and are in agreement with previously reported values for cellular methane-air flames propagating at atmospheric pressure [45].

With the source of the acceleration identified and accounted for, using Eq. 1 to analyze the radius vs time data allows the effect of aluminum combustion on the flame propagation to be separated from the effect of the cellular instability.

4.2 Physical interaction of methane and aluminum fuels

As can be seen in Fig. 6b for mixtures without excess oxygen, both mixtures containing reactive aluminum powder and inert alumina powder exhibit similar behavior at low particle loadings, with flame speeds decreasing with increasing particle concentration, agreeing with theoretical predictions which assume the particles are non-reactive. This indicates that, at low solid fuel loadings, aluminum reaction rates are much slower than the methane reaction rates and, thus, the aluminum only acts to increase the heat capacity of the mixture and slows the flame.

The behavior of the flame speed changes when the concentration reaches a value of about 100 g/m^3. Above this concentration, the flame speed stops decreasing and remains constant with respect to the particle loading, which indicates that the aluminum is reacting and contributing to the flame propagation. This observation is in qualitative agreement with a similar effect observed for Bunsen-type aluminum-methane flames [38, 39]. In the Bunsen geometry, it was observed that, at a critical concentration, an aluminum flame front forms at the tip of the Bunsen cone and propagates down the sides to form a coupled double-front structure which allows for the exchange of heat between the two combustion zones. Above this concentration, the burning velocity remains constant with further increases in aluminum concentration, similar to the flame speed behavior observed in the present experiments, indicating that the same phenomenon is also occurring in the spherical geometry.

In both geometries, spherical and Bunsen, the formation and coupling of the secondary aluminum front, in the combustion products of the primary methane flame, is only possible when the speed of the secondary aluminum flame matches the speed of the primary methane flame products. The aluminum flame speed increases with increasing solid fuel concentration, leading to the critical concentration for flame coupling [39]. The thermally coupled aluminum-methane flame at high concentrations stabilizes the burning velocity of the methane flame by conducting heat from the secondary (aluminum) to the primary (methane) reaction zones that compensates for the increased heat capacity resulting from the additional aluminum in suspension.

As can be seen in Fig. 6b, for mixtures with excess oxygen, the flame speed monotonically increases with aluminum concentration before reaching a plateau. The plateau in the flame speed at high concentrations in mixtures with excess oxygen is again indicative that an aluminum flame front is formed and coupled to the methane flame. A similar plateau in burning velocity was observed in experiments studying the same excess oxygen mixtures on the Bunsen burner and coincided with the formation of an aluminum flame which coupled to the methane flame [39].

In contrast, the present data differ not only from the mixtures without excess oxygen in the present work, but also from the results on the Bunsen burner for the same excess oxygen mixtures. On the Bunsen burner, the burning velocity initially decreased with aluminum concentrations below the critical value needed for thermal coupling, while the present set of data shows an increase in flame speed with aluminum concentration for low concentrations. The present results, combined with the previous results [39], suggest a different type of physical interaction for low aluminum concentrations than the thermal flame coupling that has been observed in previous investigations [20, 38–40].

In a spherically-expanding flame, the particles are contained within the boundary of the flame, and any delayed heat release from particles reacting behind the methane flame will increase the temperature of the gas behind the flame, leading to increased thermal expansion. This increased thermal expansion pushes on the methane flame, leading to faster observable flame speeds [17]. Similar results were recorded by Denkevitz studying fuel-lean hydrogen-air flames with varying concentrations of aluminum powder [41]. At low concentrations, the explosion takes place in two stages with two distinct peaks in the rate of pressure rise; however, as the concentration is increased, the two peaks move closer, eventually coming together resulting in a single peak. In these experiments, the addition of metal powder increased both the overall pressure rise as well as the maximum rate of pressure rise compared to the hydrogen-air mixture without any powder.

In a stabilized flame [20, 38, 39], any delayed heat release from particles reacting behind the methane flame is dissipated to the surroundings. In this configuration, the particles must react fast enough with respect to the characteristic methane flame time (i.e. the time the particles spend within the methane flame zone) in order to contribute to the flame propagation. In a spherical flame, in addition to the characteristic methane flame time, there is also the characteristic time of the entire event (i.e. the entire time the flame is propagating), and particles reacting with a characteristic time greater than that of the methane flame, but shorter than that of the total even time can still contribute to the flame propagation through the enhanced expansion effect, as discussed above. This explains why no enhancing effect was observed in the previous experiments on the Bunsen burner at low concentrations for the same excess oxygen mixtures [39].

4.3 Particle mode of combustion

Although the above discussion explains the discrepancy between the Bunsen and spherical geometries, the difference in flame speed behavior for spherical flames at low concentrations between mixtures with and without excess oxygen still requires an explanation. This difference is due to differences in the particle mode of combustion when different oxidizers are present.

As discussed in the introduction, there are two subsequent process which control the burning rate of a particle: the diffusion of oxidizer to the particle followed by the reaction at the particle [16,53]. These competing processes result in two asymptotic combustion regimes with their own distinct characteristics. If the rate of molecular transport is sufficiently fast, there will be no thermal or species gradient between the particle and the surrounding gas, and the particle will react kinetically at the Arrhenius reaction rate which depends strongly on the bulk-gas temperature: $k \propto e^{\frac{E_\mathrm{a}}{R_\mathrm{u} T_\mathrm{g}}}$. If the reaction rates are faster than the rate of diffusion, then heat will build up and oxidizing species will be depleted at the particle where the reaction is taking place. This leads to thermal and species gradients between the particle and the surrounding gas. In this case, the particle burns at a locally higher temperature where the reaction rate is largely independent of the bulk gas temperature.

The slower reaction rates and reduced amount of heat production of aluminum reacting with water vapor and carbon dioxide compared to oxygen creates the conditions for the aluminum to react in the kinetically-limited mode [16,36,53]. At low concentrations of aluminum, the particles undergo relatively slow oxidation (compared to the methane flame) at the methane flame temperature. As more aluminum is added, however, the collective effect of particles reacting and releasing heat increases the bulk-gas temperature, which in turn leads to an increase in reaction rates in a self-accelerating manner. As the concentration of aluminum is further increased, this collective effect of the particles heating the gas is also increased, and at a critical concentration, the self-heating from the particles allows the suspension of aluminum to transition from relatively slow oxidization to a rapid combustion process. Due to the exponential dependence of the Arrhenius reaction rate on temperature, and thus aluminum concentration, this transition from relatively slow oxidization to rapid combustion can occur over small concentration ranges, leading to the critical behavior evidenced in the flame speed data in Fig 6b. In this case, a critical concentration of aluminum is needed in order for the aluminum to become reactive within the system.

When aluminum can react with oxygen, the increased reaction rates and larger amount of heat release create the conditions for the particle to ignite, or transition to the diffusion-limited regime [16, 36, 53]. When this occurs, the particle burns at a locally higher temperature. This allows particles to achieve relatively fast combustion rates compared to kinetic reaction rates at the bulk-gas temperature. Therefore, even at low concentrations where the collective effect of particle heating is small, the aluminum can still react rapidly enough to contribute to the methane flame propagation. This is seen in the flame speed data in Fig 6b. At low concentrations, there is a clear deviation of the experimentally measured flame speeds from the dashed lines showing the trends assuming the particles are inert, indicating that the particles are reacting and contributing.

These assertions of different particle modes of combustion in the different oxidizing environments are also supported by recent spectroscopic measurements made on a flat flame burner using aluminum-methane fuel mixtures [54]. In the case where aluminum could only react with water vapor and carbon dioxide, the spectroscopic measurements of the aluminum vapor atomic emission lines show no evidence of self-reversal, which indicates there are no temperature gradients in the flame, which is consistent with particles burning in the kinetically-limited regime. When aluminum burned in air, where it reacts with oxygen, the emission spectroscopy did show signs of self-reversal, indicating there are temperature gradients within the flame, consistent with the particles burning the diffusion-limited regime.

Aluminum burns in the vapor-phase, and past researchers have suggested that the limiting kinetic reaction rate for aluminum combustion is the evaporation of aluminum vapor from the particle surface [36, 39], and the present experiments agree with this assertion. The boiling temperature of aluminum is 2800 K, and the adiabatic flame temperature of 0% excess oxygen mixture reaches this temperature at a concentration of 125 g/m^3, which is close to the 100 g/m^3 measured in the present experiment where the aluminum starts to react and contribute to the methane flame propagation. This suggests that the critical concentration is necessary to reach sufficient rates of aluminum evaporation to achieve rapid combustion, which is seen in the flame speed data. For the 5% and 8% excess oxygen mixtures, the concentrations at which the adiabatic flame temperature reaches the aluminum boiling temperature are 100 and 75 g/m^3, respectively; however, the particles are clearly reacting and contributing to the flame propagation at concentrations below these. In these mixtures, however, the ability for aluminum to transition to the diffusion-limited regime, allows the particle to locally reach the aluminum boiling temperature and produce sufficient amounts of aluminum vapor for rapid combustion.

Figure 8 illustrates the four different scenarios observed in the present experiment. At low metal loadings, the aluminum particles do not form a flame front and can only contribute to the methane flame propagation when excess oxygen is present due to the ignition of aluminum particles. Above a critical concentration, a second metal flame front forms and couples to the methane flame in both cases.

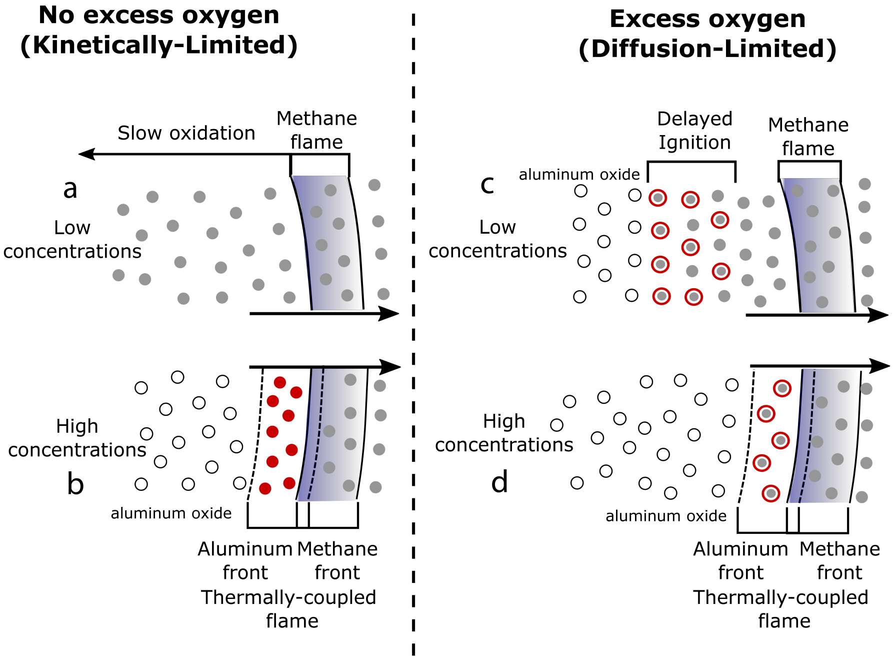

Figure 8: Particle mode of combustion and aluminum-methane flame interactions are shown. In mixtures without excess oxygen (Cases a and b), burning aluminum particles are depicted simply as red without a diffusion-flame present around the particle. In mixtures with excess oxygen (Cases c and d), the particles burn in the diffusion-limited regime with micro-diffusion flames around each particle.

5 Conclusion

The present investigation studied spherically-expanding flames in hybrid aluminum-methane fuel mixtures. This work varied aluminum concentration and oxidizer type and concentration to determine when the aluminum will be reactive within these hybrid systems. Additionally, this work examines the role of geometry in flames propagating through hybrid aluminum-methane-oxidizer mixtures and is a continuation of previous works which have studied similar hybrid mixtures on Bunsen burners [20, 38, 39], counter flow burners [54], and in quenching tubes [40].

The spherically-expanding flames were studied using transparent latex balloons which creates a near isobaric environment and permits optical access at all stages of the flame propagation, allowing for the stability of the flame propagation to be analyzed. Flames in mixtures without excess oxygen have a smooth flame surface and propagate at a steady speed. In contrast, flames in mixtures with excess oxygen have cellular structures on the surface and are found to be accelerating during the observed propagation, independent of the type of powder in suspension. Formation and growth of the cellular instabilities cause the flame to accelerate during its propagation. The radius versus time data is fit to an expression that describes the fractal growth of cellular flames, allowing the effect of aluminum combustion to be separated from the effect of the instability and enabling the unperturbed flame speed to be extracted.

For fuel-rich methane-air mixtures with no excess oxygen in the post-methane flame zone, the flame speed initially decreases with increasing aluminum concentration before reaching a plateau above a concentration around 100 g/m^3, similar to previous experiments with Bunsen flames [38, 39]. This behavior is associated with the rapid formation of a high-temperature aluminum flame which becomes thermally coupled to the methane flame and enables the aluminum-oxidation rate to be similar to that of methane. Below this critical concentration of aluminum, the aluminum undergoes oxidation at a relatively slow rate compared to the methane flame and, thus, only affects the methane flame by increasing the heat capacity of the mixture. In these mixtures, the particles react in the kinetically-limited regime, and a sufficient concentration is required for the aluminum to become reactive within the system. Furthermore, the addition of aluminum in these mixtures, even at high concentrations where the aluminum is reacting, results in flame speeds less than that of the non-metallized combustible gas mixture.

In mixtures with excess oxygen, the flame speeds monotonically increase with aluminum concentration at low concentrations before reaching a plateau for concentrations above 150 g/m^3. The ability for the particles to react rapidly at low concentrations is attributed to the particles igniting when there is oxygen with which to react. These fast reaction rates at low concentrations permit the particles to deposit energy directly in the wake of the methane flame, which causes the gases behind the methane flame to expand and push the methane flame even without becoming thermally coupled. The critical oxygen concentration at which the aluminum combustion transitions from the kinetically-limited regime to the diffusion-limited regime in hydrocarbon flame products remains an open question to be explored in future research.

The present work, along with previous studies [20, 38–40], demonstrates that thermal coupling in metal-hydrocarbon fuel mixtures is not a fuel or geometry specific phenomenon. This has important implications for improved understanding of metallized propellants, explosives, and hybrid industrial explosions, and is an area of research that requires further investigation.

Additionally, this work also shows that for spherically-expanding flames, the total time of the flame propagation, which is related to the size of the flame, introduces an additional time scale within which the the metal particles can react and contribute to the flame propagation. This has important implications for accidental explosions where very large flames are produced with event times much longer than can be produced at the laboratory scale.

References

[1] I. Glassman and R. A. Yetter. *Combustion 4th Edition*. Elsevier Inc, 2008.

[2] J. M. Bergthorson, S. Goroshin, M. J. Soo, P. Julien, J. Palecka, D. L. Frost, and D. J. Jarvis. Direct combustion of recyclable metal fuels for zero-carbon heat and power. *Applied Energy*, 160:368–382, 2015.

[3] E. W. Price. Combustion of metallized propellants. *Fundamentals of solid propellant combustion*, pages 479–513, 1984.

[4] N. H. Yen and L. Y. Wang. Reactive metals in explosives. *Propellants, Explosives, Pyrotechnics*, 37(2):143–155, 2012.

[5] W. A. Trzciński and L. Maiz. Thermobaric and enhanced blast explosives–properties and testing methods. *Propellants, Explosives, Pyrotechnics*, 40(5):632–644, 2015.

[6] R. K. Eckhoff. Prevention and mitigation of dust explosions in the process industries: A survey of recent research and development. *Journal of loss prevention in the process industries*, 9(1):3–20, 1996.

[7] R. K. Eckhoff. *Dust explosions in the process industries: identification, assessment and control of dust hazards*. Gulf professional publishing, 2003.

[8] I. Glassman. Metal Combustion Processes. Technical Report 473, United States Air Force, 1959.

[9] D. Bradley and J. H. S. Lee. On the mechanism of propagation of dust flames. In *First International Colloquium on Explosibility of Industrial Dusts. Polish Academy of Sciences, Committee for Thermodynamics and Combustion, Warszawa, Poland*, 1984.

[10] J. H. Burgoyne and L. Cohen. The effect of drop size on flame propagation in liquid aerosols. In *Proceedings of the Royal Society of London A: Mathematical, Physical and Engineering Sciences*, volume 225, pages 375–392. The Royal Society, 1954.

[11] W. Felder and A. Fontijn. High-temperature fast-flow reactor kinetic studies. the AlO/O_2 reaction near 1400 k. *The Journal of Chemical Physics*, 64(5):1977–1980, 1976.

[12] A. Fontijn, W. Felder, and J. J. Houghton. Temperature dependence of Al/O_2 and AlO/O_2 kinetics from 300 to 1700/1400 k. 16(1):871–879, 1977.

[13] A Garcia-Agreda, A. Di Benedetto, P. Russo, E. Salzano, and R. Sanchirico. Dust/gas mixtures explosion regimes. *Powder Technology*, 205(1):81–86, 2011.

[14] H. D. and Ross. *Microgravity combustion: fire in free fall.* Academic press, 2001.

[15] I. A. B. Zeldovich, G. I. Barenblatt, V. B. Librovich, and G. M. Makhviladze. *Mathematical theory of combustion and explosions.* 1985.

[16] M. Soo, S. Goroshin, J. M. Bergthorson, and D. L. Frost. Reaction of a particle suspension in a rapidly-heated oxidizing gas. *Propellants, Explosives, Pyrotechnics*, 40(4):604–612, 2015.

[17] C. K. Law. *Combustion Physics*, volume 14. 2006.

[18] M. W. Beckstead. Correlating aluminum burning times. *Combustion, Explosion and Shock Waves*, 41(5):533–546, 2005.

[19] E. Y. Shafirovich and U. I. Goldshleger. Combustion of magnesium particles in CO_2/CO mixtures. *Combustion Science and Technology*, 84(1-6):33–43, 1992.

[20] P. Julien, S. Whiteley, S. Goroshin, M. J. Soo, D. L. Frost, and J. M. Bergthorson. Flame structure and particle-combustion regimes in premixed methane–iron–air suspensions. *Proceedings of the Combustion Institute*, 35(2):2431–2438, 2015.

[21] S. Goroshin, D. L. Frost, J. Levine, A. Yoshinaka, and F. Zhang. Optical pyrometry of fireballs of metalized explosives. *Propellants Explosives Pyrotechnics*, 31(3):169–181, 2006.

[22] T. A. Brzustowski and I. Glassman. Spectroscopic investigation of metal combustion. *Heterogeneous Combustion*, 15:41, 1964.

[23] A. Davis. Solid propellants: the combustion of particles of metal ingredients. *Combustion and Flame*, 7:359–367, 1963.

[24] R. Friedman and A. Maček. Ignition and combustion of aluminium particles in hot ambient gases. *Combustion and flame*, 6:9–19, 1962.

[25] Y. V. Frolov, P. F. Pokhil, and V. S. Logachev. Ignition and combustion of powdered aluminum in high-temperature gaseous media and in a composition of heterogeneous condensed systems. *Combustion, Explosion, and Shock Waves*, 8(2):168–187, 1972.

[26] R. P. Wilson and F. A. Williams. Experimental study of the combustion of single aluminum particles in O_2/Ar. In *Proceedings of the Combustion Institute*, volume 13, pages 833–845. Elsevier, 1971.

[27] A. Maček. Fundamentals of combustion of single aluminum and beryllium particles. In *Proceedings of the Combustion Institute*, volume 11, pages 203–217. Elsevier, 1967.

[28] C. K. Law and F. A. Williams. Combustion of magnesium particles in oxygen-inert atmospheres. *Combustion and Flame*, 22(3):383–405, 1974.

[29] A. F. Belyaev, Y. V. Frolov, and A. I. Korotkov. Combustion and ignition of particles of finely dispersed aluminum. *Combustion, Explosion and Shock Waves*, 4(3):182–185, 1968.

[30] S. E. Olsen and M. W. Beckstead. Burn time measurements of single aluminum particles in steam and CO_2 mixtures. *Journal of Propulsion and Power*, 12(4):662–671, 1996.

[31] B. Legrand, M. Marion, C. Chauveau, I. Gokalp, and E. Shafirovich. Ignition and combustion of levitated magnesium and aluminum particles in carbon dioxide. *Combustion Science and Technology*, 165(1):151–174, 2001.

[32] R. J. Gill, C. Badiola, and E. L. Dreizin. Combustion times and emission profiles of micron-sized aluminum particles burning in different environments. *Combustion and Flame*, 157(11):2015–2023, 2010.

[33] C. Badiola and E. L. Dreizin. Combustion of micron-sized particles of titanium and zirconium. *Proceedings of the Combustion Institute*, 34(2):2237–2243, 2013.

[34] P. Bucher, R. A. Yetter, F. L. Dryer, T. P. Parr, and D. M. Hanson-Parr. Plif species and ratiometric temperature measurements of aluminum particle combustion in O_2, CO_2 and N_2O oxidizers, and comparison with model calculations. In *Proceedings of the Combustion Institute*, volume 27, pages 2421–2429. Elsevier, 1998.

[35] N. Glumac, H. Krier, T. Bazyn, and R. Eyer. Temperature measurements of aluminum particles burning in carbon dioxide. *Combustion science and technology*, 177(3):485–511, 2005.

[36] T. Bazyn, H. Krier, and N. Glumac. Evidence for the transition from the diffusion-limit in aluminum particle combustion. *Proceedings of the Combustion Institute*, 31(2):2021–2028, 2007.

[37] P. Lynch, G. Fiore, H. Krier, and N. Glumac. Gas-phase reaction in nanoaluminum combustion. *Combustion Science and Technology*, 182(7):842–857, 2010.

[38] M. Soo, P. Julien, S. Goroshin, J. M. Bergthorson, and D. L. Frost. Stabilized flames in hybrid aluminum-methane-air mixtures. *Proceedings of the Combustion Institute*, 34(2):2213–2220, 2013.

[39] P. Julien, M. Soo, S. Goroshin, D. L. Frost, J. M. Bergthorson, N. Glumac, and F. Zhang. Combustion of aluminum suspensions in hydrocarbon flame products. *Journal of Propulsion and Power*, 30(4):1047–1054, 2014.

[40] J. Palecka, P. Julien, S. Goroshin, J. M. Bergthorson, D. L. Frost, and A. J. Higgins. Quenching distance of flames in hybrid methane–aluminum mixtures. *Proceedings of the Combustion Institute*, 35(2):2463–2470, 2015.

[41] A. Denkevits and B. Hoess. Hybrid H_2/Al dust explosions in Siwek sphere. *Journal of Loss Prevention in the Process Industries*, 36:509–521, 2015.

[42] P. Julien, J. Vickery, A. Whiteley, S.and Wright, S. Goroshin, J. M. Bergthorson, and D. L. Frost. Effect of scale on freely propagating flames in aluminum dust clouds. *Journal of Loss Prevention in the Process Industries*, 36:230–236, 2015.

[43] P. Julien, J. Vickery, S. Goroshin, D. L. Frost, and J. M. Bergthorson. Freely-propagating flames in aluminum dust clouds. *Combustion and Flame*, 162(11):4241–4253, 2015.

[44] C. R. Bauwens, J. M. Bergthorson, and S. B. Dorofeev. Critical peclet numbers for the onset of darrieus-landau instability in atmospheric-pressure methane-air flames. *25 ICDERS University of Leeds*, 2015.

[45] C. R. Bauwens, J. M. Bergthorson, and S. B. Dorofeev. Experimental study of spherical-flame acceleration mechanisms in large-scale propane–air flames. *Proceedings of the Combustion Institute*, 35(2):2059–2066, 2015.

[46] C. R. Bauwens, J. M. Bergthorson, and S. B. Dorofeev. On the interaction of the darrieus–landau instability with weak initial turbulence. *Proceedings of the Combustion Institute*, 36(2):2815–2822, 2017.

[47] D. G. Goodwin. An open-source, extensible software suite for cvd process simulation. *Chemical Vapor Deposition XVI and EUROCVD*, 14(40):2003–08, 2003.

[48] D. Bradley and C. M. Harper. The development of instabilities in laminar explosion flames. *Combustion and Flame*, 99(3-4):562–572, 1994.

[49] D. Bradley, T. M. Cresswell, and J. S. Puttock. Flame acceleration due to flame-induced instabilities in large-scale explosions. *Combustion and Flame*, 124(4):551–559, 2001.

[50] O. C. Kwon, G. Rozenchan, and C. K. Law. Cellular instabilities and self-acceleration of outwardly propagating spherical flames. *Proceedings of the Combustion Institute*, 29(2):1775–1783, 2002.

[51] J. K. Bechtold and M. Matalon. Hydrodynamic and diffusion effects on the stability of spherically expanding flames. *Combustion and Flame*, 67(1):77–90, 1987.

[52] R. Thimothée, C. Chauveau, F. Halter, and I. Gökalp. Experimental investigation of the mechanisms of cellular instabilities developing on spherical two-phase flames. *Combustion Science and Technology*, 188(11-12):2026–2043, 2016.

[53] M. J. Soo, K. Kumashiro, S. Goroshin, D. L. Frost, and J. M. Bergthorson. Thermal structure and burning velocity of flames in non-volatile fuel suspensions. *Proceedings of the Combustion Institute*, 36(2):2351–2358, 2017.

[54] M. Soo, S. Goroshin, N. Glumac, K. Kumashiro, J. Vickery, D. L. Frost, and J. M. Bergthorson. Emission and laser absorption spectroscopy of flat flames in aluminum suspensions. *Combustion and Flame*, 180:230–238, 2017.